NEURAL REGENERATION RESEARCH
www.nrronline.org

Research Article

Neural progenitor cells derived from fibroblasts induced by small molecule compounds under hypoxia for treatment of Parkinson's disease in rats

Yu Guo[1, #], Yuan-Yuan Wang[1, #], Ting-Ting Sun[1, #], Jia-Jia Xu[1], Pan Yang[1], Cai-Yun Ma[1, 2], Wei-Jun Guan[2], Chun-Jing Wang[1], Gao-Feng Liu[1, *], Chang-Qing Liu[1, 3, *]

https://doi.org/10.4103/1673-5374.355820

Date of submission: February 25, 2022

Date of decision: June 18, 2022

Date of acceptance: July 30, 2022

Date of web publication: October 10, 2022

From the Contents

Graphical Abstract

Rat neural progenitor cells derived from fibroblasts induced by small molecule compounds improve neurological deficits in Parkinsonian rats

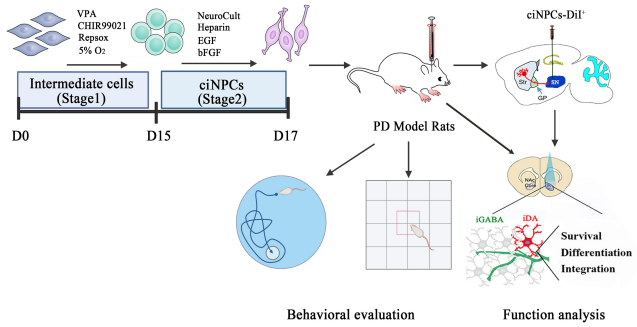

Abstract

Neural progenitor cells (NPCs) capable of self-renewal and differentiation into neural cell lineages offer broad prospects for cell therapy for neurodegenerative diseases. However, cell therapy based on NPC transplantation is limited by the inability to acquire sufficient quantities of NPCs. Previous studies have found that a chemical cocktail of valproic acid, CHIR99021, and Repsox (VCR) promotes mouse fibroblasts to differentiate into NPCs under hypoxic conditions. Therefore, we used VCR (0.5 mM valproic acid, 3 μM CHIR99021, and 1 μM Repsox) to induce the reprogramming of rat embryonic fibroblasts into NPCs under a hypoxic condition (5%). These NPCs exhibited typical neurosphere-like structures that can express NPC markers, such as Nestin, SRY-box transcription factor 2, and paired box 6 (Pax6), and could also differentiate into multiple types of functional neurons and astrocytes *in vitro*. They had similar gene expression profiles to those of rat brain-derived neural stem cells. Subsequently, the chemically-induced NPCs (ciNPCs) were stereotactically transplanted into the substantia nigra of 6-hydroxydopamine-lesioned parkinsonian rats. We found that the ciNPCs exhibited long-term survival, migrated long distances, and differentiated into multiple types of functional neurons and glial cells *in vivo*. Moreover, the parkinsonian behavioral defects of the parkinsonian model rats grafted with ciNPCs showed remarkable functional recovery. These findings suggest that rat fibroblasts can be directly transformed into NPCs using a chemical cocktail of VCR without introducing exogenous factors, which may be an attractive donor material for transplantation therapy for Parkinson's disease.

Key Words: cell reprogramming; cell transplantation; hypoxia; neural progenitor cells; neurological function; Parkinson's disease; small molecule compounds; substantia nigra

Introduction

Parkinson's disease (PD) is the second-most common neurodegenerative disorder that affects 2–3% of the global population aged ≥ 65 years (Kalia and Lang, 2015; Poewe et al., 2017). Resting tremor, bradykinesia, rigidity, and postural instability are the major motor manifestations of PD (Lubbe and Morris, 2014; Michel et al., 2016). The main pathology of PD is the progressive loss of dopaminergic (DA) neurons in the substantia nigra (SN) that project to the striatum and the formation of α-synuclein-containing Lewy bodies (Tang et al., 2017; Parmar et al., 2020). The underlying molecular pathogenesis involves multiple pathways and mechanisms: α-synuclein proteostasis, mitochondrial function, oxidative stress, calcium homeostasis, axonal transport, and neuroinflammation (Barker et al., 2015; Liu and Cheung, 2020). Motor symptoms in PD are treated using levodopa, dopamine agonists, and monoamine oxidase and catechol-O-methyl-transferase inhibitors (Armstrong and Okun, 2020; Abdelrahman and Gabr, 2022). However, over time, these medications lose efficacy and result in side effects, such as dyskinesia, hallucinations, impulse control disorders, and other psychiatric problems (Huot et al., 2013; Barker et al., 2015; Parmar et al., 2020). Because the loss of DA neurons is the main hallmark of PD, cell transplantation strategies have been considered potential therapies (Yasuhara et al., 2017). Several studies have demonstrated that different types of stem cells can survive and differentiate into DA neurons after transplantation into PD animal models, which subsequently alleviated the clinical symptoms of PD (Liu et al., 2013; Monni et al., 2014; Dhivya and Balachandar, 2017).

Compared with embryonic stem cells (ESCs) and induced pluripotent stem cells (iPSCs), neural progenitor cells (NPCs) have the advantages of less immune rejection, less tumorigenicity, and better stability (Ke et al., 2019; D'Souza et al., 2021; Han et al., 2021). Several studies have indicated that neural transplantation using NPCs can ameliorate neurological deficits and restore dysfunctional neural circuitry in animal models (Mine et al., 2018; Xu et al., 2020; Zhang et al., 2021). However, cell therapy based on NPC transplantation for treating nervous system diseases is limited by the

[1]School of Laboratory Medicine, School of Life Sciences, Bengbu Medical College, Bengbu, Anhui Province, China; [2]National Germplasm Resource Center for Domestic Animals, Institute of Animal Science, Chinese Academy of Agricultural Science, Beijing, China; [3]Department of Neuroscience, University of Connecticut Health Center, Farmington, CT, USA
***Correspondence to:** Chang-Qing Liu, PhD, lcq7813@bbmc.edu.cn; Gao-Feng Liu, MS, lgfmy@bbmc.edu.cn.
https://orcid.org/0000-0002-1059-6528 (Chang-Qing Liu)
#These authors contributed equally to this work.

Funding: *This study was supported by the National Natural Science Foundation of China, No. 81771381 (to CQL); Anhui Provincial Key Research and Development Project, Nos. 2022e07020030 (to CQL), 2022e07020032 (to YG); Science Research Project of Bengbu Medical College, No. 2021byfy002 (to CQL); the Natural Science Foundation of the Higher Education Institutions of Anhui Province, No. KJ2021ZD0085 (to CJW); and the Undergraduate Innovative Training Program of China, Nos. 202110367043 (to CQL), 202110367044 (to YG).*

How to cite this article: *Guo Y, Wang YY, Sun TT, Xu JJ, Yang P, Ma CY, Guan WJ, Wang CJ, Liu GF, Liu CQ (2023) Neural progenitor cells derived from fibroblasts induced by small molecule compounds under hypoxia for treatment of Parkinson's disease in rats. Neural Regen Res 18(5):1090-1098.*

inability to acquire sufficient quantities of NPCs (Tang et al., 2018). Although conventional strategies for NPC generation, such as cell primitive derivation from brain tissues or induction from pluripotent cells (e.g., ESCs and iPSCs), have been established over the past several years, they are time-consuming and have been associated with ethical and clinical safety concerns (Cheng et al., 2014). In comparison with the insertion of exogenous genes, chemical compound-mediated cell reprogramming offers numerous advantages, such as no genetic modification, higher safety, lower cost, and greater efficiency (Hou et al., 2013; Tang and Cheng, 2017). The use of small molecule compounds to directly reprogram somatic cells to differentiate into neural stem cells or NPCs not only reduces tumorigenicity but also improves the efficiency of differentiation, offering promise for cell replacement repair and gene transfer therapy for central nervous system damage and related diseases (Tang and Cheng, 2017; Zhou et al., 2020). In addition to neural stem cells and/or NPCs, several other important target cells have been successfully generated using this method, including neurons (Zhang et al., 2015; Yin et al., 2019), Schwann cells (Thoma et al., 2014), pluripotent stem cells (Hou et al., 2013), and cardiomyocytes (Cao et al., 2016). However, despite these achievements, the functions and mechanisms underlying chemical-induced cell reprogramming remain poorly understood.

NPCs can be successfully generated from mouse fibroblasts via a chemical cocktail of VCR (valproic acid, CHIR99021, and Repsox) under hypoxia (Cheng et al., 2014). Valproic acid is a histone deacetylase inhibitor that promotes fibroblast reprogramming, and it can inhibit senescence during reprogramming by downregulating p16 and p21 pathways and suppressing cell cycle arrest to improve reprogramming efficiency (Zhai et al., 2015). CHIR99021 is a glycogen synthase kinase 3 (GSK-3) inhibitor that promotes cell self-renewal and maintains cell pluripotency by stabilizing downstream effectors (Yang et al., 2020). Repsox is a transforming growth factor-β (TGF-β) receptor kinase inhibitor that inhibits the TGF-β/suppressor of mothers against decapentaplegic signaling pathway and induces fibroblast reprogramming (Guo et al., 2021). In this study, we aimed to directly convert rat embryonic fibroblasts (REFs) into chemically-induced NPCs (ciNPCs) via small molecule compounds under hypoxic conditions (5% oxygen [O_2]) and stereotactically transplanting ciNPCs into the SN of 6-hydroxydopamine (6-OHDA)-lesioned parkinsonian rats to detect their functional effects *in vivo*.

Methods

Animals

Overall, 30 specific-pathogen-free 8-week-old healthy male Sprague-Dawley rats weighing 180–220 g and pregnant rats were provided by the Animal Experimental Center of Anhui Medical University (license No. SCXK [Lu] 2019-0003). The rats were reared in a pathogen-free room under a controlled temperature of 26°C. The stocking density was ≤ 4 animals/box, and the relative humidity was controlled at 40–70% on a 12-hour light/dark cycle with ad libitum access to food and water. The use of animals and all experimental procedures were approved by the Institutional Animal Care and Use Committee (IACUC) for Ethics of Bengbu Medical College (approval No. 2020-025) on April 3, 2020. All experiments were designed and reported according to the Animal Research: Reporting of *In Vivo* Experiments guidelines (Percie du Sert et al., 2020).

Isolation and culture of REFs and NSCs

Primary REFs were mechanically isolated and cultured from day 16–18 rat embryos (E16–18) as previously described (Guo et al., 2021). Briefly, after pregnant rats were anesthetized by subcutaneous injection of 3% pentobarbital sodium (50 mg/kg, Merck KGaA, Darmstadt, Germany) into the lateral lower abdomen, embryonic tissues without the head, limbs, visceral tissues, gonads, or vertebral column were cut into pieces and trypsinized. Isolated REFs were expanded until passage 3 (P3) and used for subsequent experiments. REFs were maintained in high-glucose Dulbecco's modified Eagle's medium (H-DMEM), supplemented with 10% fetal bovine serum (Gibco, Thermo Fisher Scientific, Waltham, MA, USA), 1% GlutaMax (Life Technologies, Carlsbad, CA, USA), 1% non-essential amino acids, 100 U/mL penicillin, and 0.1 mg/mL streptomycin, and cultured at 37°C in a 5% carbon dioxide (CO_2) humidified atmosphere. Rat NSCs were derived from E16 mouse embryos and expanded in a neural expansion medium (NEM; NeuroCult Basal medium, STEMCELL Technologies, Vancouver, BC, Canada), supplemented with 2% B27, 20 ng/mL epidermal growth factor (EGF), and 20 ng/mL basic fibroblast growth factor (bFGF).

Generation of ciNPCs induced by REFs

To chemically induce the conversion of REFs into ciNPCs, the initial REFs at P3 cultured in H-DMEM supplemented with 10% fetal bovine serum for 48 hours were transferred into a knockout serum replacement medium (Thermo Fisher Scientific), which contained knockout Dulbecco's modified Eagle's medium (DMEM), 15% knockout serum replacement, 1% non-essential amino acids, 1% GlutaMax, 1% sodium pyruvate, 0.1 mM β-mercaptoethanol, 1000 U/mL leukemia inhibitory factor, 0.5 mM valproic acid (Sigma-Aldrich, Merck KGaA, Darmstadt, Germany), 3 μM CHIR99021 (Sigma-Aldrich), and 1 μM Repsox (Selleckchem, Houston, TX, USA). Cells were cultured at 37°C under 5% CO_2 and 21% or 5% O_2 (hypoxia) for 15 days. The medium-containing chemical compounds were changed every 5 days to enable the REFs to become intermediate cells (Cheng et al., 2014). The compact cell colonies formed by the REFs were then detected using alkaline phosphatase kits (Beyotime Biotechnology, Nantong, China) following the manufacturer's protocols. After digestion with 0.25% trypsin-ethylene diamine tetraacetic acid, the cells were replated onto a low adhesion plate and replaced with NEM (NeuroCult Basal medium, 30 ng/mL heparin + 20 ng/mL EGF + 20 ng/mL bFGF). The suspended neurospheres were observed for 2 days, and the free-floating clusters were collected, which were referred to as passage 1 (P1) ciNPCs. Neurospheres are recommended to be passaged when they reach 100–150 μm in diameter (typically 5–8 days after plating).

CiNPC immunofluorescent staining

Cells cultured on coverslips were fixed with 4% paraformaldehyde for 18 minutes, followed by permeabilization with 0.2% Triton X-100 for 10 minutes, and blocked with 1% bovine serum albumin and 10% normal donkey serum for 1 hour at 20°C. The following primary antibodies were used to incubate with the samples overnight at 4°C: mouse anti-β-III-tubulin (Tuj1, 1:300, Abcam, Cambridge, MA, USA, Cat# ab7751, RRID: AB_306045), mouse anti-Nestin (1:300, Abcam, Cat# ab6142, RRID: AB_305313), rabbit anti-paired box6 (Pax6, 1:50, Abcam, Cat# ab5790, RRID: AB_305110), rabbit anti-synaptophysin (1:200, Abcam, Cat# ab32594, RRID: AB_778204), rabbit anti-neuronal nuclear antigen (1:200, Abcam, Cat# ab177487, RRID: AB_2532109), chicken anti-microtubule-associated protein 2 (1:500, Abcam, Cat# Ab5392, RRID: AB_2138153), rabbit anti-SRY-box transcription factor 2 (Sox2; 1:300, Cat# 3579S, RRID: AB_2195767, CST, Boston, MA, USA), and rabbit anti-glial fibrillary acidic protein (GFAP; 1:50, Cat# MO22136, #RRID: AB_2341541, Neuromics, Edina, MN, USA). Cells were then incubated with appropriate secondary antibodies (Alexa Fluor 488-conjugated donkey anti-rabbit immunoglobulin G [IgG], 1:500, Invitrogen, Carlsbad, CA, USA, Cat# A21206, RRID: AB_2535792; Cy3-conjugated donkey anti-rabbit, 1:1000, Jackson Immunoresearch, West Grove, PA, USA, Cat# 711-165-150, RRID: AB_2340813; or Cy3-conjugated goat anti-chicken IgG, 1:500, Jackson Immunoresearch, Cat# 103-165-155, RRID: AB_2337386) for 1 hour at 20°C. The nuclei were counterstained with 4′,6-diamidino-2-phenylindole dihydrochloride (DAPI) for 15 minutes. The immunofluorescence results for the expression of marker proteins and the proportion of positive cells were observed under a multiphoton laser scanning microscope (Olympus, FV1200MPE SHARE, Tokyo, Japan).

Quantitative polymerase chain reaction and western blot assay

Total RNAs were extracted from the cells using the Trizol reagent (Invitrogen) following the manufacturer's protocols. Quantitative real-time polymerase chain reaction (PCR) was carried out using TB Green Premix Ex Taq II (TaKaRa Bio, Dalian, China) and analyzed with QuantStudio 6 Flex Thermocycler (Applied Biosystems, Carlsbad, CA, USA). The primer sequences for quantitative PCR (qPCR) were synthesized by Sangon Biotech (Shanghai, China) and presented in **Table 1**. PCR amplifications were carried out under the following conditions: one cycle of initial denaturation for 30 seconds at 95°C, followed by 40 cycles of denaturation for 10 seconds at 95°C and 20 seconds at 60°C.

Table 1 | **Sequences of primers for quantitative polymerase chain reaction analysis**

Gene	Primer sequences (5'–3')	Product size (bp)
4-Oct	Forward: CGT TCT CTT TGG AAA GGT GTT C	314
	Reverse: ACA CTC GAA CCA CAT CCC TC	
Sox2	Forward: GCA GTA CAA CTC CAT GAC	70
	Reverse: CGA GTA GGA CAT GCT GTA	
Nestin	Forward: TGC AGC CAC TGA GGT ATC TG	1062
	Reverse: CAG TTC CCA CTC CTG TGG TT	
GAPDH	Forward: GTA TGT CGT GGA GTC TAC	150
	Reverse: GAG TTG TCA TAT TTC TCG TGG T	

GAPDH: Glyceraldehyde-3-phosphate dehydrogenase; Oct4: organic cation/carnitine transporter 4; Sox2: SRY-box transcription factor 2.

For western blotting, the equivalent amounts of proteins (40 μg) from each sample were separated by sodium dodecyl sulfate-polyacrylamide gel electrophoresis, transferred to a polyvinylidene difluoride membrane (0.45 μM, Millipore, Billerica, MA, USA), and immunoblotted overnight at 4°C with the primary antibodies of rabbit anti-Pax6 (1:500, Cat# ab5790, RRID: AB_305110, Abcam), mouse anti-Nestin (1:800, Cat# ab6142, RRID: AB_305313, Abcam), rabbit anti-Sox2 (1:500, Cat# 3579S, RRID: AB_2195767, CST), and mouse anti-β-actin (1: 1000, Cat# sc-47778, RRID: AB_626632, Santa Cruz Biotechnology, Santa Cruz, CA, USA). Immunoreactive proteins were incubated with horseradish peroxidase-labeled secondary antibodies (goat anti-mouse IgG, 1:5000, Cat# 115-035-003, RRID: AB_10015289, or goat anti-rabbit IgG, 1:5000, Cat# 111-035-003, RRID: AB_2313567, Jackson Immunoresearch) for 1 hour at 20°C. The protein bands were then visualized using Clarity Western ECL Blotting Substrates (Bio-Rad Laboratories, Hercules, CA, USA) and quantified using Software Quantity One version 1-D (Bio-Rad Laboratories).

Differentiation of ciNPCs *in vitro*

P5 or P13 ciNPCs derived from the rat fibroblasts were cultured in NEM with EGF (20 ng/mL), bFGF (20 ng/mL), and heparin (30 ng/mL). For general neural differentiation, 20,000 ciNPCs were plated onto poly-L-ornithine hydrobromide (PLO)/laminin-coated 24-well plates in N2B27 medium (DMEM:F12, 1% N2, 2% B27). For neuronal differentiation, ciNPCs were plated onto PLO/laminin-coated coverslips in neural differentiation medium (neural basal medium, 2% B27, 1% N2, 10 ng/mL brain-derived neurotrophic factor [BDNF], 10 ng/mL

glial cell line-derived neurotrophic factor [GDNF], 10 ng/mL insulin-like growth factor 1 [IGF-1], 1 μM cyclic adenosine monophosphate [cAMP], and 200 μM ascorbic acid) (Cheng et al., 2014; Zhu et al., 2021). The expression of neuronal markers was monitored at the indicated time points.

Bioinformatics analysis of RNA sequencing verification

Total RNAs were extracted from six samples (i.e., REFs, rat NSCs, REFs induced in 15 days by VCR under hypoxia [H15], REFs induced in 15 days by VCR under normoxia [N15], ciNPCs induced under hypoxia [HPC], and ciNPCs induced under normoxia [NPC]) using the Arcturus PicoPure RNA Isolation Kit (Applied Biosystems, Foster City, CA, USA). RNA integrity was assessed using an Agilent 2100 Bioanalyzer (Agilent Technology, Palo Alto, CA, USA). Six complementary DNA libraries were constructed at Sangon Biotech Co., Ltd. (Shanghai, China) and were subjected to 125 bp end sequencing using the Illumina HiSeq 2500 platform (Illumina, San Diego, CA, USA). Raw reads were filtered to obtain high-quality clean reads. DESeq (an R package, http://www.rproject.org/) was used to evaluate differentially expressed genes (DEGs) in the six groups (Anders and Huber, 2010). The overlapping area of DEGs in each group was summarized by the Venn diagram package in R. Similar expression profiles across the six groups were analyzed via principal component analysis using the R vegan (version 2.0-10) package (http://www.usadellab.org/cms/) (Bolger et al., 2014). A global genome heat map was generated and hierarchical cluster and scatter plot analyses were performed using the gplots (version 2.17.0) and DEGseq (version 1.26.0) packages in R, respectively. Gene ontology (GO) classifications were compared between the up- and downregulated unigenes using the Web GO Annotation Plot method (Ye et al., 2018). ClusterProfiler (version 3.8.1) from the R software package was used to annotate the pathways related to the DEGs and compare these against the Kyoto Encyclopedia of Genes and Genomes (KEGG) database (https://www.kegg.jp/kegg/) (Yu et al., 2012). Gene sequences were annotated with the Swiss-Prot, National Center for Biotechnology Information (NCBI) non-redundant protein sequence (NR), and Karyotic Ortholog Group (KOG) databases using the NCBI Blast$^+$ software (version 2.60; https://blast.ncbi.nlm.nih.gov/Blast.cgi) (Altschul et al., 1997) and the KEGG database using the KEGG Automatic Annotation Serve (KAAS) software (version 2.1; http://www.genome.jp/tools/kaas) (Moriya et al., 2007). The results of the annotated genes in the four databases were displayed in a Venn diagram.

PD modeling

Endogenously produced estrogen is neuroprotective in females, whereas in males, gonadal factors increase striatal 6-OHDA toxicity and facilitate the establishment of a PD rat model (Gillies et al., 2004; Reglödi et al., 2006). The male rats were randomly divided into two groups; 10 rats were used as negative controls (i.e., the healthy group). The remaining 20 rats were anesthetized by intraperitoneal injection of 3% pentobarbital sodium (50 mg/kg) and fixed on a stereotaxic apparatus (Narishige Scientific Instrument Lab., Tokyo, Japan). Eight microliters of 6-OHDA solution (5 mg/mL, dissolved in 0.2% ascorbate saline; Sigma-Aldrich) were unilaterally infused into the right SN at the following two coordinates at a rate of 0.5 μL/min: anterior –4.4 mm (from the bregma), lateral –1.2 mm (from the bregma), ventral –7.8 mm (from the dura); and anterior –4.0 mm (from the bregma), lateral –0.8 mm (from the bregma), and ventral –8.0 mm (from the dura). The needle was maintained for an additional 8 minutes before retraction (Guo et al., 2022). Following drug infusion, the skin incision was closed with stainless steel wound clips.

Behavioral assessment of the parkinsonian rat model

Apomorphine-induced behavioral rotation

Two weeks after the 6-OHDA injection, the rats were injected intraperitoneally with 0.5 mg/kg apomorphine (APO; Sigma-Aldrich), and the rotational behavior contralateral to the lesion side was recorded quantitatively for 30 minutes to assess motor dysfunction. Those that exhibited more than 210 ipsilateral rotations/30 minutes were selected as parkinsonian model rats for transplantation (Liu et al., 2008; Sundberg et al., 2013). In addition, all behavioral assessments were evaluated 2, 4, and 8 weeks after cell transplantation.

Open field test

The rats were placed in the central grid of the open-field apparatus and their movement was videotaped for the duration of the trial. The total distance traveled during each trial was automatically recorded and analyzed by the Ethovision XT 10.1S system (Noldus, Leesburg, Netherlands) over 5 minutes to detect the locomotive activity of the rats (Goffin et al., 2011). Zone maps were generated by tracing the path of the rats in the open field.

Water maze assay

A Morris water-maze tracking system (temperature of 19–22°C, TME Technology, Chengdu, China) was used to evaluate the motor coordination ability of the rats. The rats were placed into the pool and allowed a maximum of 10 minutes to mount the platform freely, which was captured automatically by the camera. The Ethovision XT 10.1S system (Noldus) automatically recorded and analyzed the total distance traveled, the time spent searching for the platform, and the speed of finding the platform.

Rotarod test

Three rats were detected simultaneously on the three-station rotarod apparatus to assess the motor coordination of the rats (SANS, Nanjing, China). The test processed a constant 300 revolutions per minute for 30 minutes, and each animal completed three trials. The number of turns and the time spent on the rod were recorded, and the trial was automatically paused when the rat fell off the rod or ran for 30 minutes.

Transplantation of ciNPCs into the right SN of parkinsonian rats

P3 ciNPCs were dissociated into single cells by TrypLE (Gibco) and stained by Cell Tracker CM-DiI (1 μg/μL, Invitrogen) for 30 minutes at 37°C. After rinsing the cells once with phosphate-buffered saline, the cell suspension was resuspended with H-DMEM in 1.25×10^4/μL for transplantation. The ciNPCs were unilaterally transplanted into the right SN of each parkinsonian model rat using the same two stereotaxic coordinates as those used in the PD model. Twenty PD model rats were randomly divided into ciNPC (n = 10) and vehicle groups (n = 10). At each site, 8 μL of cell suspension containing 1.0×10^5 ciNPCs was injected into the PD rats using a Hamilton microsyringe (Reno, NV, USA) at a rate of 0.5 μL/min (ciNPCs group). The remaining PD rats were injected with 8 μL serum-free H-DMEM in the same manner (vehicle group).

The rats were perfused with 0.9% NaCl, followed by 4% paraformaldehyde, under deep anesthesia by intraperitoneal injection of 3% pentobarbital sodium (50 mg/kg) 8 weeks after cell transplantation. Briefly, the anesthetized rats were placed on the dissection table and their limbs were fixed. The epidermis and muscle from the ventral midline to xiphoid midline were cut to expose the heart. The heart was slightly clamped with hemostatic forceps, and the perfusion needle was inserted directly from the apex 2–3 mm into the aorta. The right atrial appendage was cut, and normal saline was quickly infused until the organs turned white, followed by 4% formaldehyde. If sufficient paraformaldehyde is perfused, the limbs of the rats will twitch continuously and become rigid. The brains were post-fixed for 24 hours in 4% paraformaldehyde and subsequently cryoprotected in 10%, 20%, and 30% sucrose solution at 4°C for 24–48 hours.

Whole perfused brains were sectioned into 12-μm thick coronal sections using a microtome cryostat (Leica, CM-1850, Wetzlar, Germany) and mounted on gelatin-coated glass slides. To detect cell survival, differentiation, and function of the transplanted ciNPCS, the cryosections were stained with primary antibodies overnight at 4°C: mouse anti-Tuj1 (1:300, Cat# ab7751, RRID: AB_306045), rabbit anti-postsynaptic density-95 (PSD95, 1:300, CST, Cat# 2507S, RRID: AB_561221), rabbit anti-γ-aminobutyric acid (GABA, 1:300, Sigma-Aldrich, Cat# A2052, RRID: AB_477652), and rabbit anti-GFAP (1:300, Cat# MO22136, RRID: AB_2341541, Neuromics). After secondary antibody incubation conjugated to Alexa Fluor 488 (donkey anti-rabbit IgG, 1:500, Cat# A21206, RRID: AB_2535792, or donkey anti-mouse IgG, 1:500, Cat# A21202, RRID: AB_141607, Invitrogen) for 1 hour at 20°C, the immunofluorescence results were observed under a multiphoton laser scanning microscope (Olympus, FV1200MPE SHARE, Tokyo, Japan). Meanwhile, the perfused brains were paraffin-embedded and sectioned into 30-μm thick sections using a microtome. The sections were then routinely incubated with rabbit anti-tyrosine hydroxylase (TH, 1:300, Cat# ab112, RRID: AB_297840, Abcam) antibody overnight at 4°C. After three rinses in Dulbecco's phosphate-buffered saline, horseradish peroxidase-labeled goat anti-rabbit secondary antibody (1:1000, Cat# 111-035-003, RRID: AB_2313567, Jackson Immunoresearch) was added and incubated for 1 hour at 20°C. The sections were then stained with 3,3′-diaminobenzidine tetrahydrochloride (Servicebio, Wuhan, China). Additionally, for the histopathology examination, 3-μm thick paraffin sections were dewaxed in xylene, rehydrated via decreasing concentrations of ethanol, washed in phosphate-buffered saline, and stained with hematoxylin-eosin staining solution (Servicebio). After staining, the sections were dehydrated via increasing concentrations of ethanol and xylene. The results of the survival and number of TH$^+$ cells for the TH-3,3′-diaminobenzidine and HE staining were detected by whole-brain scanning using the Nikon Imaging system (Nikon DS-U3, Tokyo, Japan) and the CaseViewer 2.0 software (3DHISTECH Ltd., Budapest, Hungary).

Statistical analysis

Sample sizes were not predetermined statistically; however, our sample sizes are similar to those reported in previous publications (Mendes-Pinheiro et al., 2018; Mine et al., 2018). No animals or data points were excluded from the analysis. The experiments were not randomized, and investigators were not blinded to allocation during the experiments or outcome assessments. All quantitative data are presented as means ± standard errors of the mean for at least three independent experiments. Statistical comparisons between two groups were performed using Student's t-test. $P < 0.05$ was considered statistically significant. For comparison between more than two groups, we used one-way analyses of variance followed by Tukey's *post hoc* tests. The GraphPad Prism 7.00 software(GraphPad Software, San Diego, CA, USA, www.graphpad.com) was used for all statistical analyses and the generation of graphs.

Results

Induction of ciNPCs from REFs by VCR under physiological hypoxia

Primary cultured fibroblasts were initially mixed with epithelial cells, and because of their rapid growth, fibroblasts gradually replaced epithelial cells after 2–4 passages of subculture. The induction of ciNPCs from REFs by small molecular compound VCR under physiological hypoxia (5% O_2) underwent two major developmental stages (**Figure 1A**). Step-by-step cell morphological changes throughout the induction process are shown in **Figure 1B**. During the first stage, the intermediate cells were chemically induced. The cellular morphology of many REFs changed to a bipolar shape, similar to that of NPCs during this process (**Figure 1C**). Compact cell colonies were observed in REFs cultured at 5% O_2 15 days after VCR, and 1000 U/mL leukemia inhibitory

factor was added to the culture medium. Approximately 30 compact cell colonies emerged from 1 × 10^5 REFs, and most colonies (90%) expressed a high level of alkaline phosphatase (**Figure 1D** and **E**). The second stage was lineage-specific induction. Intermediary compact cell colonies were digested with 0.25% trypsin-ethylene diamine tetraacetic acid, replated onto low adhesion six-well plates, and cultured in suspension in NEM containing heparin, EGF, and bFGF under normoxic conditions. A large number of free-floating neurospheres were formed 2 days after passage. We collected these free-floating clusters, which we defined as P1 ciNPCs. Additionally, the expression levels of neural-related genes and proteins, including Sox2, Pax6, and Nestin, were significantly enhanced by qPCR and western blot analyses (**Figure 1F** and **G**).

Proliferation and self-renewal of ciNPCs

The ciNPC neurospheres induced by VCR under hypoxia were phase-bright and became more spherical as their size increased. The results of immunofluorescence staining showed that the ciNPC neurospheres inoculated on sterile glass slides pre-coated with PLO and laminin had typical neurosphere-like structures that expressed NPC markers, including Nestin, Sox2, and Pax6 (**Figure 2A** and **B**). Subsequently, these ciNPC neurospheres were further cultured in suspension to examine whether they possess two fundamental characteristics of NPCs: proliferation and self-renewal. After 13 passages cultured in NEM, the ciNPCs maintained good neurosphere formation and proliferation ability, with no change in morphology. In the different generations (i.e., P1, P3, P5, and P13), the ciNPCs cultured in an adherent monolayer showed no significant changes in morphology or growth state, which was extremely similar to rat NPCs (**Figure 2C**). Moreover, no significant differences in the size or number of neurospheres were found between P10 and P3 ciNPCs (**Figure 2D**). Next, we cultured P13 ciNPCs in an adherent monolayer and found that more than 93% of all ciNPCs were stained positive for Nestin, Sox2, and Pax6 individually, and approximately 90% of ciNPCs expressed Nestin/Sox2 or Nestin/Pax6 (**Figure 3A** and **B**).

CiNPCs show multipotency *in vitro*

The third fundamental characteristic of NPCs is their developmental multipotency (Cheng et al., 2014). The multipotency of ciNPCs was assessed by culturing cells under neuronal or glial differentiation conditions *in vitro*. We found that 14 days after induction, most cells of P3 ciNPCs became GFAP-positive with astrocyte-like morphology in neural basal medium with N2 and B27 (**Figure 4A**). Over 60% of ciNPCs became Tuj1-positive with neuron-like morphology in neural basal medium with B27, N2, BDNF, GDNF, IGF-1, cAMP, and ascorbic acid (**Figure 4B**). Moreover, neuronal nuclear antigen and postsynaptic microtubule-associated protein 2 double-positive cells with neuron-like morphology were found in the culture (**Figure 4C**). After being cultured in a neural differentiation medium for 3 weeks, Tuj1-positive mature neurons began to express presynaptic membrane marker synaptophysin (**Figure 4D**).

Gene expression profiling of ciNPCs resembles that of NPCs

To access the exact identity of ciNPCs, we extracted messenger RNA from the NSC, REF, HPC, NPC, H15, and N15 groups and compared the global gene expression patterns of these cells using microarray analysis. Pearson's correlation coefficients for the clustering analysis of the six groups showed that HPC and NPC were aggregated at one branch, and H15 and N15 were aggregated at another branch (**Figure 5A**). Similarly, HPC and NPC had similar expression profiles, whereas H15 was shown to be similar to N15 via principal component analysis (**Figure 5B**). The global genome heat map and the hierarchical cluster (**Figure 5C**) and scatter plot analyses (**Figure 5D**) revealed a significant difference between NSC and REF and high similarity between HPC, NPC, and control NSC. Although P1 ciNPCs retained some residual fibroblast epigenetic memory, several differences from rat NSCs remained, and the similarities between ciNPCs and NSCs gradually increased in subsequent generations.

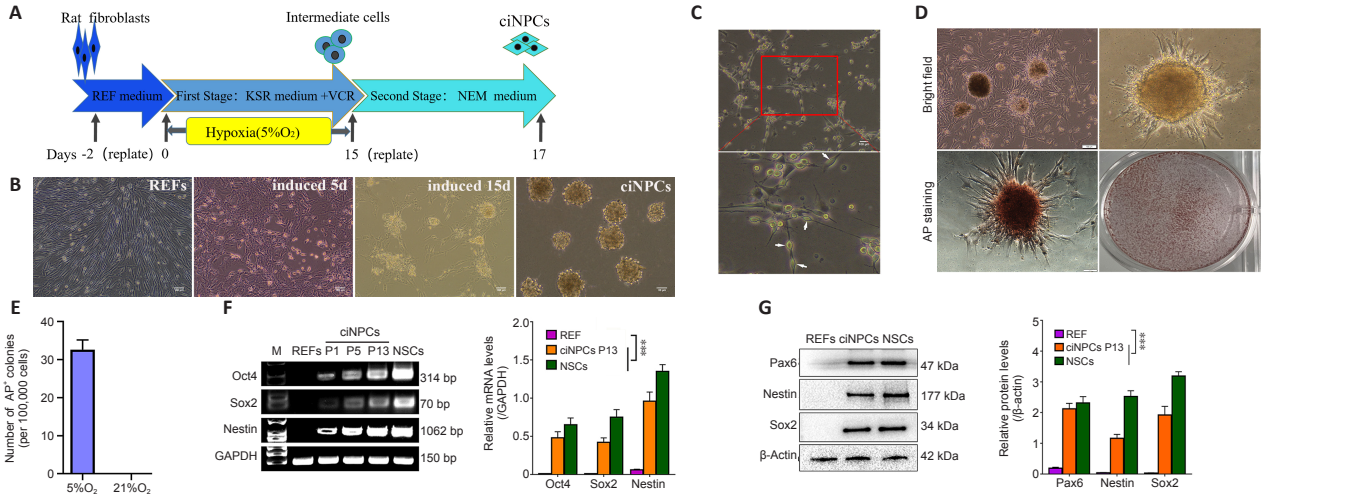

Figure 1 | Induction of chemically-induced neural progenitor cells (ciNPCs) from rat embryonic fibroblasts (REFs) by a chemical cocktail of valproic acid, CHIR99021, and Repsox (VCR) under a physiological hypoxic condition.

(A) Scheme of the experimental strategy for induction of ciNPCs from rat fibroblasts. The initial fibroblasts were plated in Dulbecco's modified Eagle's medium; this day was defined as "day −2." (B) Changes in cell morphology at different stages of the induction process. The cultured REFs were spindle-shaped. Obvious cell aggregation was observed 5 days after induction, and compact cell colonies were observed 15 days after induction. A large number of free-floating neurospheres formed 2 days after passage. Scale bars: 100 μm. (C) NPC-like bipolar cells induced from VCR-treated REFs are indicated by white arrows. (D) Induction of AP-positive compact cell colonies by VCR under hypoxia. (E) Bars represent the number of colonies per 100,000 cells initially plated. (F) Relative expression levels of neural-specific genes were monitored by quantitative polymerase chain reaction. Data are expressed as means ± SEM (n = 3). ***P < 0.001, *vs*. REFs (one-way analysis of variance followed by Tukey's *post hoc* test). (G) Expression of neural-specific genes was detected by western blotting. AP: Alkaline phosphatase; ciNPCs: chemical-induced rat neural progenitor cells; GAPDH: glyceraldehyde-3-phosphate dehydrogenase; KSR: knockout serum replacement; NEM: neural expansion medium; NSCs: neural stem cells; Oct4: organic cation/carnitine transporter4; P: passage; Pax6: paired box6; REFs: rat embryonic fibroblasts; Sox2: SRY-box transcription factor 2.

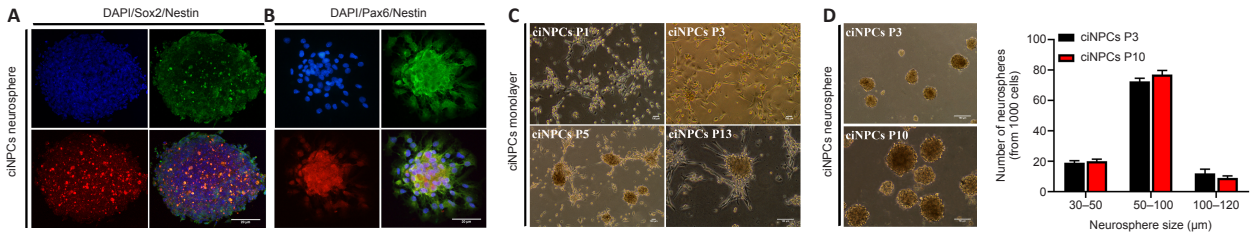

Figure 2 | Proliferation and self-renewal of chemically-induced neural progenitor cells (ciNPCs).

(A) The induced ciNPCs were positive for NPC markers Nestin (red, stained by Cy3) and SRY-box transcription factor 2 (Sox2; green, stained by Alexa Fluor 488). Scale bar: 20 μm. (B) The induced ciNPCs were positive for NPC marker Nestin (red, stained by Cy3) and paired box 6 (Pax6; green, stained by Alexa Fluor 488). The nuclei were counterstained with 4′,6-diamidino-2-phenylindole dihydrochloride (DAPI; blue). (C) Representative images of ciNPCs at passages 1, 3, 5, and 13 (P1, P3, P5, P13) cultured in an adherent monolayer show no significant changes in morphology or growth state. (D) Neurospheres of ciNPCs at P3 versus those at P10 cultured in suspension. Statistical analysis showed no significant differences in the size or number of neurospheres between P10 and P3 ciNPCs. Scale bars: 100 μm (above), 50 μm (below). Data are expressed as means ± SEM (n = 8): ciNPCs: Chemical-induced rat neural progenitor cells; DAPI: 4′,6-diamidino-2-phenylindole dihydrochloride; Pax6: paired box6; Sox2: SRY-box transcription factor 2.

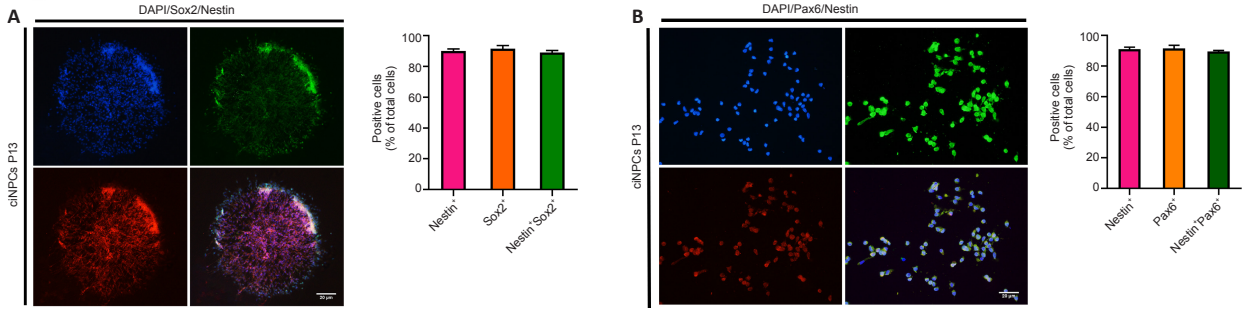

Figure 3 | **Expression of Nestin, paired box 6 (Pax6), and SRY-box transcription factor 2 (Sox2) was visualized by immunostaining P13 chemically-induced neural progenitor cells (ciNPCs).**

(A, B) Representative images for Nestin (red, stained by Cy3)/Sox2 (green, stained by Alexa Fluor 488) (A) or Nestin (red, stained by Cy3)/Pax6 (green, stained by Alexa Fluor 488) (B). Nuclei were counterstained with 4′,6-diamidino-2-phenylindole dihydrochloride (DAPI; blue). The numbers of positive cells are illustrated in the right panel. Scale bars: 20 μm. Data are expressed as means ± SEM (n = 6). ciNPCs: Chemical-induced rat neural progenitor cells; DAPI: 4′,6-diamidino-2-phenylindole dihydrochloride; P13: passage 13; Pax6: paired box6; Sox2: SRY-box transcription factor 2.

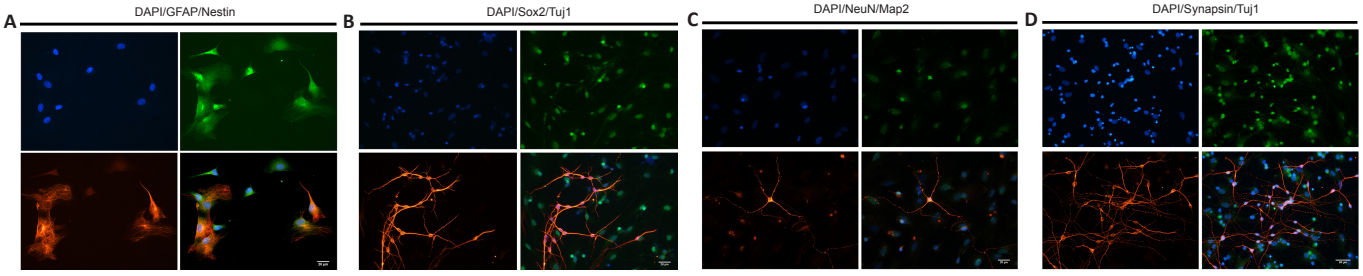

Figure 4 | **Multipotency of rat embryonic fibroblast (REF)-chemically-induced neural progenitor cells (ciNPCs) *in vitro*.**

(A) REF-ciNPCs differentiated into astrocytes and expressed the astrocyte marker glial fibrillary acidic protein (GFAP; green, stained by Alexa Fluor 488). (B) REF-ciNPCs expressed neuronal markers tubulin (Tuj1; red, stained by Cy3) and SRY-box transcription factor 2 (Sox2; green, stained by Alexa Fluor 488) after being cultured in a neural differentiation medium. (C) REF-ciNPCs expressed neuronal markers microtubule-associated protein 2 (Map2; red, stained by Cy3) and NeuN (green, stained by Alexa Fluor 488) after being cultured in a neural differentiation medium. (D) REF-ciNPCs expressed neuronal markers Tuj1 (red, stained by Cy3) and Synapsin (green, stained by Alexa Fluor 488) after being cultured in a neural differentiation medium for 3 weeks. Scale bars: 20 μm. ciNPCs: Chemical-induced rat neural progenitor cells; DAPI: 4′,6-diamidino-2-phenylindole dihydrochloride; Map2: microtubule-associated protein 2; NeuN: neuronal nuclear antigen; REFs: rat embryonic fibroblasts; Sox2: SRY-box transcription factor 2; Tuj1: β-III-tubulin.

The GO and KEGG analyses showed that upregulated DEGs were mainly enriched in the neuroactive ligand-receptor interaction, whereas the phosphatidylinositol 3′-kinase-Akt signaling pathway was the most enriched pathway for downregulated DEGs. Furthermore, 30 enriched pathways comprising upregulated genes were further classified into four categories: metabolism, environmental information processing, cellular processes, and organismal systems. Thirty enriched pathways comprising downregulated genes were classified into five categories: metabolism, genetic information processing, environmental information processing, cellular processes, and organismal systems (**Figure 5E** and **F**). To determine the molecular mechanism underlying the reprogramming of fibroblast cells into ciNPCs, we performed KOG, NCBI NR, Swissport, and KEGG analyses for the DEGs among the six groups (**Figure 5G**). The shared core targets of ciNPCs from different batches and control NSCs comprised 1645 genes (**Figure 5H**), which were primarily related to neural processes and cell morphogenesis. Most DEGs involved in various metabolic processes and signaling pathways were significantly upregulated in ciNPCs (**Figure 5E**), indicating that reprogramming induced changes in the metabolism of cells by altering multiple signaling pathways. However, DEGs involved in the cell cycle, DNA replication, and mismatch repair were significantly downregulated in ciNPCs (**Figure 5F**), suggesting that reprogramming inhibited the cell proliferation of ciNPCs. In addition, we found that the expression of neural-specific genes, such as Sox2, Pax6, and Ascl1, was significantly upregulated in ciNPCs and was comparable to that of NSCs.

Transplantation of ciNPCs improves the behavioral function of parkinsonian rat models

A total of 30 adult male rats were divided into three groups (**Figure 6A**). Two weeks after 6-OHDA injection (**Figure 6B**), the rats exhibited tail-pressing, arching, and sniffing behaviors, and they displayed more than 210 continuous ipsilateral rotations/30 minutes to the side contralateral to the injury in the APO-induced rotation test, which was the main criterion for PD model rats. The right SN of the PD rat model was damaged after the 6-OHDA lesion (**Figure 6C**). CiNPCs-DiI$^+$ were stereotaxically injected into the right SN of the 6-OHDA rats at the two coordinates shown in **Figure 6D** and **E**, and the total number of cells ranged from 0.8 to 1.2 × 10^5 cells/graft (n = 10). Four weeks after the transplantation of ciNPCs-DiI$^+$, the APO-induced rotation behavior of the transplanted rats was slightly reduced, although it did not differ significantly from that of the PD model rats. However, the rotation behavior gradually decreased with time, reaching 242.5 ± 22.5 (n = 8) turns 8 weeks after transplantation (**Figure 6F** and **G**). Moreover, there was a significant reduction in rotation behavior in the ciNPC group (**Figure 6G**), indicating that the transplanted cells required time to induce functional recovery *in vivo*. The motor coordination ability of the ciNPC group was improved as assessed by the rotarod test (P < 0.05; **Figure 6H** and **I**). Furthermore, the rats that underwent ciNPC transplantation were more excited and active than those in the vehicle group, and the total distance traveled in the open field test was significantly increased (P < 0.01; **Figure 6J** and **K**). In the water maze, the grafted rats spent significantly less time seeking the platform than the vehicle group (**Figure 6L** and **M**).

Survival and function of ciNPCs in the host SN of parkinsonian rat models

Whole-brain hematoxylin-eosin staining results revealed that the number of cells in the 6-OHDA-lesioned area of PD rats was significantly lower than that of the healthy control group, and the cells were arranged in a disorderly manner. However, numerous ciNPCs grafts were observed and shown to have survived well in the brain environment of PD rats 8 weeks after transplantation (**Figure 7A**). The TH-3,3′-diaminobenzidine tetrahydrochloride staining of the whole-brain scan revealed significantly fewer TH$^+$ cells in the brain of the vehicle group than in the brain of the healthy control group. However, a large number of TH$^+$ cells were observed in the engraftment area of ciNPCs and the area surrounding the PD rat brain SN 8 weeks after transplantation. Microscopic imaging showed significantly higher TH labeling in the transplanted putamen than in the vehicle group putamen, which indicated that the transplanted putamen recovered well from the transplantation of ciNPCs. Moreover, there were significantly more viable DA neurons in the putamen of the ciNPC group than in the vehicle group (**Figure 7B**).

Transplanted ciNPCs formed obvious graft regions 2 weeks after implantation and migrated from the graft area 8 weeks after transplantation (**Figure 7C**). In addition, the area of cell distribution from the grafted area was significantly larger at 8 weeks than at 2 weeks after transplantation. These CM-DiI labeled cells survived for at least 8 weeks and migrated long distances (2.0–2.5 mm) from the graft site into the surrounding brain tissue and damaged area to play a repairing role (**Figure 7C**). Moreover, the engrafted ciNPCs gave rise to various functional neurons around and within the graft 8 weeks after transplantation and expressed the neuronal marker β-III-tubulin, the glutamatergic neuronal marker PSD95, and the glial marker GFAP (**Figure 7D**) (Gao et al., 2017). Most CM-DiI labeled cells expressed neuronal markers PSD95, GABA, and TH 8 weeks after transplantation (**Figure 7E**). These data demonstrate that ciNPCs can differentiate into functional neurons and astrocytes in the host SN. Many grafted cells were positive for TH staining, and TH$^+$ fiber outgrowth was also detected from the graft site. Furthermore, TH$^+$ cell clusters were scattered throughout the graft and integrated into the host brain tissue (**Figure 7F**). Given that TH is a marker of DA neurons (Parmar et al., 2020), our findings suggest that transplanted ciNPCs can differentiate into DA neurons in the host brain microenvironment. Moreover, the expression of synaptophysin was significantly increased after ciNPC transplantation, and numerous DiI-positive cells were positive for synaptophysin staining (**Figure 7G**). We also found a large number of synaptophysin-positive and DiI-negative patches adjacent to the transplanted ciNPCs, which indicated that host-derived presynaptic terminals made contact with ciNPCs-derived neurons to form mature synapses (**Figure 7G**). Importantly, no tumor formation was observed in any of the grafted rats after ciNPC transplantation.

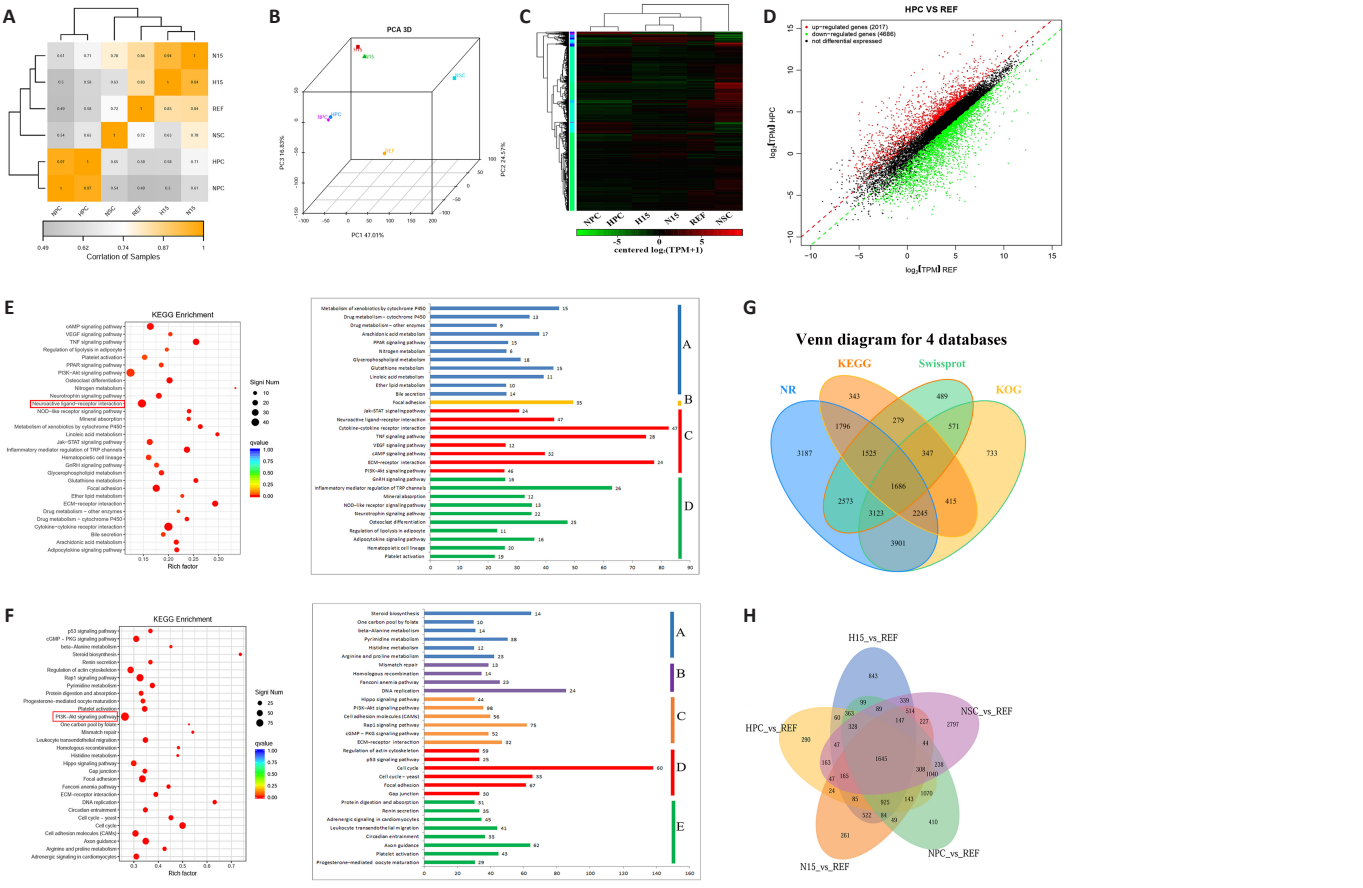

Figure 5 | **Enriched pathways consisting of differentially expressed genes (DEGs) in the six libraries using RNA-sequencing.**
(A) Heatmap analysis of the correlation of expression profiles among the six groups. (B) Principal component analysis of six samples to detect similarities. (C) Heatmap and hierarchical clustering of genes with significance from microarray analysis data revealed a significant difference between chemically-induced neural progenitor cells (ciNPCs) and rat embryonic fibroblasts (REFs). (D) Digital expression levels of DEGs in ciNPCs induced under hypoxia (HPC) and REFs. Red points indicate upregulated DEGs, and green points indicate downregulated DEGs. (E) Thirty enriched pathways comprising upregulated genes were further classified into four categories between HPC and REF. (F) Thirty enriched pathways comprising downregulated genes were further classified into five categories between HPC and REF. (G) Venn diagram for four databases showing 1686 overlapping genes in the six groups. (H) Venn diagram illustrating the overlap of expression changes identified in HPC, ciNPCs induced under normoxia (NPC), REFs induced in 15 days by VCR under hypoxia (H15), REFs induced in 15 days by VCR under normoxia (N15), and NSC compared with the expression changes in REFs. ciNPCs: Chemical-induced rat neural progenitor cells; DEGs: differentially expressed genes; H15: REFs induced by VCR 15 days under hypoxia; HPC: ciNPCs induced under hypoxia; KEGG: Kyoto Encyclopedia of Genes and Genomes; KOG: Karyotic Ortholog Groups; N15: REFs induced by VCR 15 days under normoxia; NPC: ciNPCs induced under normoxia; NR: NCBI non-redundant protein sequences; NSCs: neural stem cells; REFs: rat embryonic fibroblasts; VCR: valproic acid, CHIR99021, and Repsox.

Discussion

Induction of ciNPCs from REFs by small molecule compound VCR

To our knowledge, this is the first study to show that direct lineage-specific conversion of REFs into NPCs can be achieved using a chemical cocktail of VCR, which had a significant effect on dyskinesias in PD rats *in vivo*. REFs were reprogrammed into ciNPCs in two major stages. The first stage was chemical induction, in which fibroblasts were reprogrammed into intermediate cells to avoid the risk of tumorigenicity due to the activation of pluripotency during the induction process. The hypoxia induction time increased to 15 days, the number of compact cell colonies of intermediate cells increased significantly, and most colonies were positively stained for alkaline phosphatase. The second stage was lineage-specific induction. The intermediate cells were digested with 0.25% trypsin-ethylene diamine tetraacetic acid and inoculated on low adhesion plates. After 2 days of culturing in normoxic suspension, we obtained the first generation of chemically-induced rat NPC neurospheres. These ciNPCs were highly similar to rat brain-derived embryonic NPCs in terms of morphology, self-renewal ability, proliferation ability, and multipotency *in vitro*.

Although master transcription factors are considered the main determinants of specific cell characteristics (Caiazzo et al., 2011; Pfisterer et al., 2011; Kim et al., 2014; Wang et al., 2015), small molecule compounds can activate the expression of these genes and play important roles. This has led to small molecule compounds receiving increased attention in somatic cell reprogramming and transdifferentiation research (Li et al., 2015; Tang and Cheng, 2017; Qin et al., 2018). The inhibition of histone deacetylases, TGF-β, and GSK-3 by the diverse inhibitors of VCR enabled the conversion of differentiated fibroblast cells into intermediary cells under physiological hypoxic conditions. Moreover, this process was accompanied by the activation of endogenous Sox2 expression. Therefore, these three essential signaling pathways may facilitate the desired transition by regulating the expression of Sox2-controlled genes (Cheng et al., 2014). The REF-ciNPC neurospheres had a typical neurosphere-like structure, expressed NPC markers of Nestin, Sox2, and Pax6, possessed the typical characteristics of NPCs, and maintained good spheroidization ability after the serial passage to P13. Furthermore, RNA-seq analysis revealed that the expression of genes known to be regulated by these pathways in ciNPCs was significantly different from that in REFs, which further supported the idea that activation of a defined set of genes via these pathways is critical for the successful transition of REFs to NPCs. The direct conversion of cells avoided the need for cells to pass through the pluripotent stem cell state, which prevented the formation of tumors after being transplanted into the brain or other organs. However, the precise regulatory mechanisms remain to be investigated.

Transplanted ciNPCs differentiate into functionally active neurons and integrate into the brain of parkinsonian rats

The PD rat model was established by injecting 6-OHDA directly into the SN of rats to destroy DA neurons. The number of rotations induced by APO in PD rats was closely associated with the degree of DA depletion in the SN (Liu et al., 2008; Zenchak et al., 2020). In terms of generating DA neurons, iPSCs are very similar to ESCs in that they respond to the same differentiation cues and generate mature cells with highly similar functional properties (Kikuchi et al., 2017). Although undifferentiated ESCs and iPSCs can improve the behavior of 6-OHDA-lesioned rats, they also carry the risk of tumor formation and teratomas *in vivo* (Fong et al., 2010; Yasuda et al., 2018). Nevertheless, NPCs have been shown to survive well, restore motor function in primate PD models, and avoid the formation of tumors (Gonzalez et al., 2016). Moreover, several previous studies have demonstrated that grafted NPCs differentiate into TH^+ neurons (DA neurons) and improve the motor behavior of PD mice and rats (Mine et al., 2018; Yuan et al., 2018; Qian et al., 2020).

In the present study, the transplantation of REF-ciNPCs into the SN of 6-OHDA-lesioned rats significantly improved motor functional recovery based on PD behavioral and neurological tests assessed via the open field, Morris

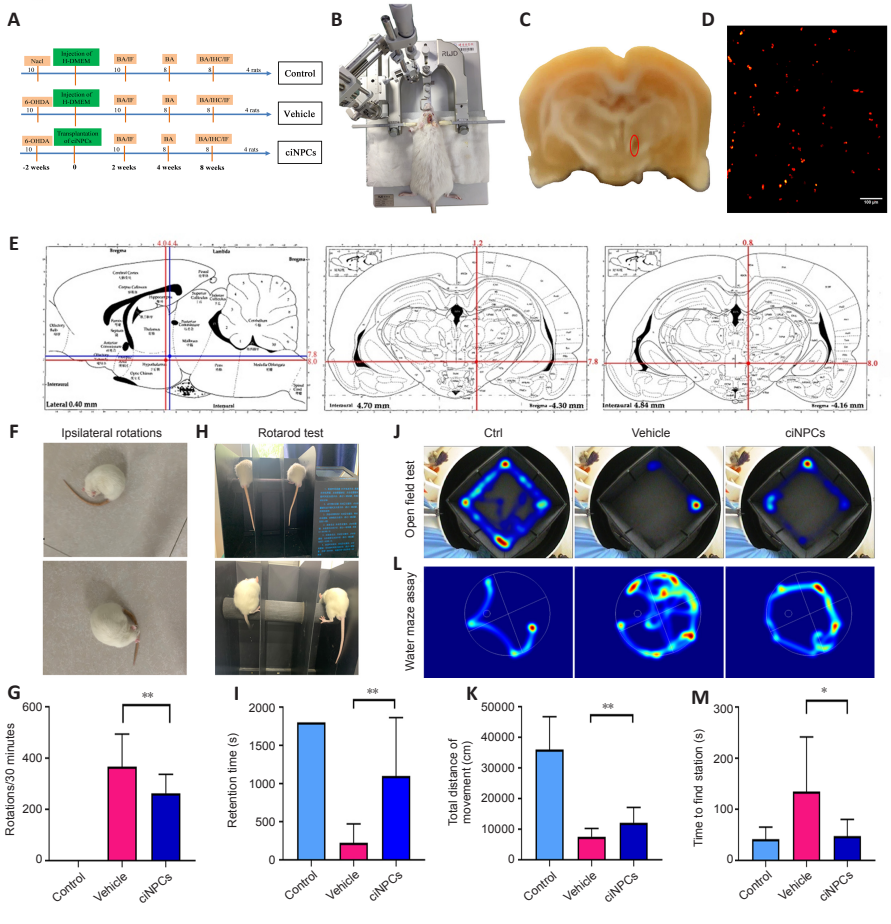

Figure 6 | Chemically-induced neural progenitor cells (ciNPCs) significantly ameliorated the behavioral deficits of 6-hydroxydopamine (6-OHDA)-lesioned rats.
(A) A flow chart of the experimental design and animal groups. (B) Experimental rats were fixed onto a stereotaxic apparatus. (C) Injury by 6-OHDA induced in the right substantia nigra (SN; red circle) in the Parkinson's disease rat model. (D) CiNPCs (red) were labeled with Cell Tracker CM-DiI before transplantation. Scale bars: 100 μm. (E) CiNPCs were stereotactically transplanted into the right SN of each model rat, ipsilateral to the lesion at two sites at the labeled coordinates (intersection of the two blue and two red lines). (F) Ipsilateral rotation in the apomorphine test. (G) Ipsilateral rotation evaluation of the three groups. (H) Rotarod test on the rotarod apparatus. (I) Rotarod test evaluation of the three groups. (J) Heat maps of the open field test showed that the total distance traveled was significantly higher in the ciNPC group than in the vehicle group. (K) Total distances traveled in the three groups. (L) Heat maps of the Morris water maze assay showed that the rats in the ciNPC group spent less time seeking the platform than the vehicle group. (M) Time to find the station by the rats in the three groups. Data are expressed as means ± SEM (n = 10). *P < 0.05, **P < 0.01, *vs.* vehicle group (one-way analysis of variance followed by Tukey's *post hoc* test). 6-OHDA: 6-Hydroxydopamine; APO: apomorphine; BA: behavioral analysis; ciNPCs: chemical-induced rat neural progenitor cells; Ctrl: control; H-DMEM: high glucose-Dulbecco's modified Eagle's medium; IF: immunofluorescence; IHC: immunohistochemistry; SN: substantia nigra.

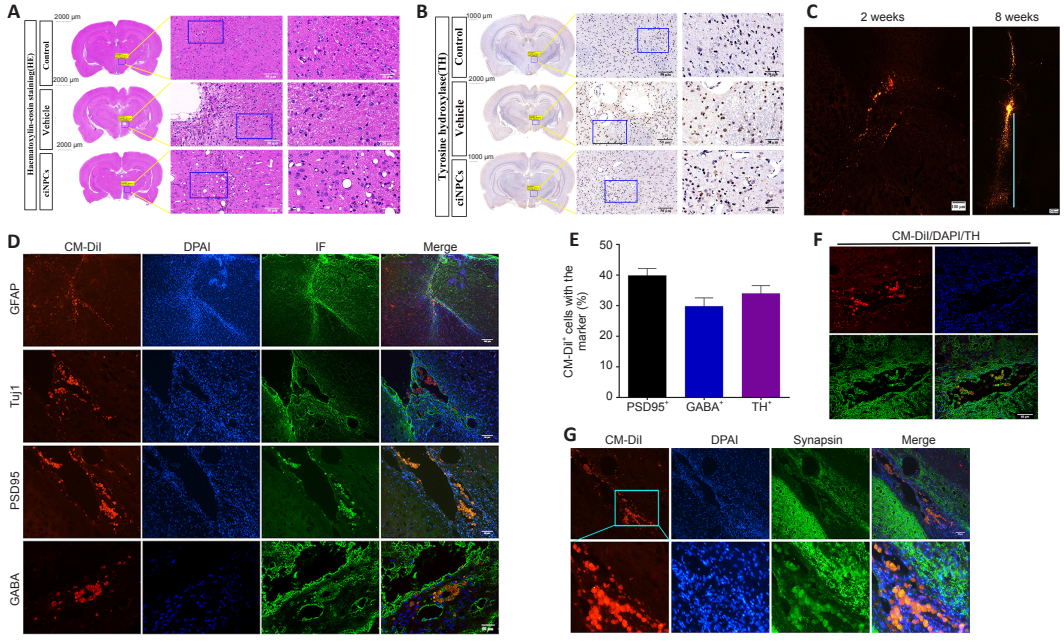

Figure 7 | Survival and integration of transplanted chemically-induced neural progenitor cells (ciNPCs) in the host brains of the parkinsonian rat models.
(A) Representative images of whole-brain scans with hematoxylin and eosin staining. The number of cells in the 6-hydroxydopamine (6-OHDA)-lesioned area of the Parkinson's disease (PD) rats was significantly lower than that of the healthy control group, and numerous ciNPCs grafts were observed in the lesion area of PD rats 8 weeks after transplantation. (B) The tyrosine hydroxylase (TH) intensity of the 6-OHDA-lesioned rats was significantly increased after ciNPC transplantation by TH-3,3′-diaminobenzidine staining. (C) CM-DiI labeled cells formed obvious graft regions after 2 weeks and migrated 2.5–3.0 mm from the graft site 8 weeks after transplantation. Scale bar: 100 μm. The blue line represents the migration distance of the transplanted cells from the graft site. (D) Grafted ciNPCs cells differentiated into various functional neurons *in vivo*, which expressed tubulin (Tuj1), postsynaptic density (PSD95), γ-aminobutyric acid (GABA), and glial fibrillary acidic protein (GFAP). Scale bars: 50 μm. (E) A proportion of CM-DiI labeled cells expressed PSD95, GABA, and TH 8 weeks after transplantation. Data are expressed as mean ± SEM (n = 6) and were analyzed by one-way analysis of variance followed by Tukey's *post hoc* test. (F) TH^+ cells integrated into the host brain 8 weeks after transplantation. Robust survival of dopamine neurons with outgrowth integration into the host putamen was observed. Scale bar: 50 μm. (G) Transplanted cells expressed the synapse marker synaptophysin (green, stained by Alexa Fluor 488) during the process. Scale bar: 50 μm. ciNPCs: Chemical-induced rat neural progenitor cells; DAB: 3,3′-diaminobenzidine; DAPI: 4′,6-diamidino-2-phenylindole dihydrochloride; GABA: γ-aminobutyric acid; GFAP: glial fibrillary acidic protein; IF: immunofluorescence; PD: Parkinson's disease; PSD95: postsynaptic density-95; TH: tyrosine hydroxylase; Tuj1: β-III-tubulin.

water maze, and rotarod tests. Moreover, the immunofluorescence results showed that ciNPC grafts can differentiate into various functional neurons and glial cells in the host brain microenvironment to improve the neurological deficits of 6-OHDA lesioned rats, such as the number of surviving $GFAP^+$, $GABA^+$, $PSD95^+$, and TH^+ cells. Furthermore, these functional neurons may be responsible for modifying the balance of excitatory and inhibitory signals in the striatum to promote behavioral recovery in PD model rats. The maturation of and increase in donor-derived TH^+ cells (DA neurons) and the synaptic formation between donor-derived cells and the host brain may contribute to functional recovery and behavioral improvement. More importantly, some of the transplanted cells differentiated into astrocytes, which play essential supportive roles for neurons and are considered active participants in the development and plasticity of dendritic spines and synapses (Blanco-Suárez et al., 2017; Zhao et al., 2020). Therefore, the behavioral improvements observed in PD rats are likely related to the combined effects of the striatal DA neurons, GABAergic neurons, and astrocytes derived from the transplanted ciNPCs. Further work is required to clarify whether these functional neurons that differentiate from ciNPCs are capable of making functional synaptic connections with neurons and integrating with the host circuitry in PD rat models. Moreover, given our small sample size of 30 rats and the analysis methods used, further investigation of the therapeutic effects of ciNPCs on motor dysfunction in PD rats is required.

In summary, we used a step-by-step induction method to directly induce rat fibroblasts to transdifferentiate into NPCs under hypoxic conditions using small molecule compounds VCR, which were highly similar to rat brain-derived embryonic NPCs. We demonstrated that ciNPCs grafts can survive and differentiate into different types of functional cells to improve neurological deficits in 6-OHDA lesioned PD rats; thus, they may serve as attractive donor material for neuroscience research and the treatment of neurodegenerative diseases.

Author contributions: *Study conception and design: WJG, GFL, CQL; animal studies and data analysis: JJX; other experiments and data collection: YG, YYW, TTS; statistical analysis: PY; manuscript draft: CYM, CJW. All authors revised the manuscript and approved the final manuscript.*
Conflicts of interest: *The authors claim that there are no conflicts of interest.*
Availability of data and materials: *High-throughput RNA sequencing data is available at the Sequence Read Archive (SRA) database (https://www.ncbi.nlm.nih.gov/sra) under the accession No. PRJNA793062.*

Open peer reviewers: *Jeffrey Schweitzer, Massachusetts General Hospital, USA; Jose Miguel Laffita-Mesa, Karolinska University Hospital, Sweden.*
Additional file: *Open peer review reports 1 and 2.*

References

Abdelrahman SA, Gabr MT (2022) Emerging small-molecule therapeutic approaches for Alzheimer's disease and Parkinson's disease based on targeting microRNAs. Neural Regen Res 17:336-337.

Altschul SF, Madden TL, Schäffer AA, Zhang J, Zhang Z, Miller W, Lipman DJ (1997) Gapped BLAST and PSI-BLAST: a new generation of protein database search programs. Nucleic Acids Res 25:3389-3402.

Anders S, Huber W (2010) Differential expression analysis for sequence count data. Genome Biol 11:R106.

Armstrong MJ, Okun MS (2020) Diagnosis and treatment of Parkinson disease: a review. JAMA 323:548-560.

Barker RA, Drouin-Ouellet J, Parmar M (2015) Cell-based therapies for Parkinson disease-past insights and future potential. Nat Rev Neurol 11:492-503.

Blanco-Suárez E, Caldwell AL, Allen NJ (2017) Role of astrocyte-synapse interactions in CNS disorders. J Physiol 595:1903-1916.

Bolger AM, Lohse M, Usadel B (2014) Trimmomatic: a flexible trimmer for Illumina sequence data. Bioinformatics 30:2114-2120.

Caiazzo M, Dell'Anno MT, Dvoretskova E, Lazarevic D, Taverna S, Leo D, Sotnikova TD, Menegon A, Roncaglia P, Colciago G, Russo G, Carninci P, Pezzoli G, Gainetdinov RR, Gustincich S, Dityatev A, Broccoli V (2011) Direct generation of functional dopaminergic neurons from mouse and human fibroblasts. Nature 476:224-227.

Cao N, Huang Y, Zheng J, Spencer CI, Zhang Y, Fu JD, Nie B, Xie M, Zhang M, Wang H, Ma T, Xu T, Shi G, Srivastava D, Ding S (2016) Conversion of human fibroblasts into functional cardiomyocytes by small molecules. Science 352:1216-1220.

Cheng L, Hu W, Qiu B, Zhao J, Yu Y, Guan W, Wang M, Yang W, Pei G (2014) Generation of neural progenitor cells by chemical cocktails and hypoxia. Cell Res 24:665-679.

D'Souza GX, Rose SE, Knupp A, Nicholson DA, Keene CD, Young JE (2021) The application of in vitro-derived human neurons in neurodegenerative disease modeling. J Neurosci Res 99:124-140.

Dhivya V, Balachandar V (2017) Cell replacement therapy is the remedial solution for treating Parkinson's disease. Stem Cell Investig 4:59.

Fong CY, Gauthaman K, Bongso A (2010) Teratomas from pluripotent stem cells: a clinical hurdle. J Cell Biochem 111:769-781.

Gao L, Guan W, Wang M, Wang H, Yu J, Liu Q, Qiu B, Yu Y, Ping Y, Bian X, Shen L, Pei G (2017) Direct generation of human neuronal cells from adult astrocytes by small molecules. Stem Cell Reports 8:538-547.

Gillies GE, Murray HE, Dexter D, McArthur S (2004) Sex dimorphisms in the neuroprotective effects of estrogen in an animal model of Parkinson's disease. Pharmacol Biochem Behav 78:513-522.

Goffin D, Allen M, Zhang L, Amorim M, Wang IT, Reyes AR, Mercado-Berton A, Ong C, Cohen S, Hu L, Blendy JA, Carlson GC, Siegel SJ, Greenberg ME, Zhou Z (2011) Rett syndrome mutation MeCP2 T158A disrupts DNA binding, protein stability and ERP responses. Nat Neurosci 15:274-283.

Gonzalez R, Garitaonandia I, Poustovoitov M, Abramihina T, McEntire C, Culp B, Attwood J, Noskov A, Christiansen-Weber T, Khater M, Mora-Castilla S, To C, Crain A, Sherman G, Semechkin A, Laurent LC, Elsworth JD, Sladek J, Snyder EY, Redmond DE, Jr., et al. (2016) Neural stem cells derived from human parthenogenetic stem cells engraft and promote recovery in a nonhuman primate model of Parkinson's disease. Cell Transplant 25:1945-1966.

Guo Y, Zhu H, Li X, Ma C, Sun T, Wang Y, Wang C, Guan W, Liu C (2021) Multiple functions of reversine on the biological characteristics of sheep fibroblasts. Sci Rep 11:12365.

Guo Y, Guan Y, Zhu H, Sun T, Wang Y, Huang Y, Ma C, Emery R, Guan W, Wang C, Liu C (2022) Therapeutic function of iPSCs-derived primitive neuroepithelial cells in a rat model of Parkinson's disease. Neurochem Int 155:105324.

Han F, Liu Y, Huang J, Zhang X, Wei C (2021) Current approaches and molecular mechanisms for directly reprogramming fibroblasts into neurons and dopamine neurons. Front Aging Neurosci 13:738529.

Hou P, Li Y, Zhang X, Liu C, Guan J, Li H, Zhao T, Ye J, Yang W, Liu K, Ge J, Xu J, Zhang Q, Zhao Y, Deng H (2013) Pluripotent stem cells induced from mouse somatic cells by small-molecule compounds. Science 341:651-654.

Huot P, Johnston TH, Koprich JB, Fox SH, Brotchie JM (2013) The pharmacology of L-DOPA-induced dyskinesia in Parkinson's disease. Pharmacol Rev 65:171-222.

Kalia LV, Lang AE (2015) Parkinson's disease. Lancet 386:896-912.

Ke M, Chong CM, Su H (2019) Using induced pluripotent stem cells for modeling Parkinson's disease. World J Stem Cells 11:634-649.

Kikuchi T, Morizane A, Doi D, Magotani H, Onoe H, Hayashi T, Mizuma H, Takara S, Takahashi R, Inoue H, Morita S, Yamamoto M, Okita K, Nakagawa M, Parmar M, Takahashi J (2017) Human iPS cell-derived dopaminergic neurons function in a primate Parkinson's disease model. Nature 548:592-596.

Kim SM, Flaßkamp H, Hermann A, Araúzo-Bravo MJ, Lee SC, Lee SH, Seo EH, Lee SH, Storch A, Lee HT, Schöler HR, Tapia N, Han DW (2014) Direct conversion of mouse fibroblasts into induced neural stem cells. Nat Protoc 9:871-881.

Li X, Zuo X, Jing J, Ma Y, Wang J, Liu D, Zhu J, Du X, Xiong L, Du Y, Xu J, Xiao X, Wang J, Chai Z, Zhao Y, Deng H (2015) Small-molecule-driven direct reprogramming of mouse fibroblasts into functional neurons. Cell Stem Cell 17:195-203.

Liu CQ, Hu DN, Liu FX, Chen Z, Luo JH (2008) Apomorphine-induced turning behavior in 6-hydroxydopamine lesioned rats is increased by histidine and decreased by histidine decarboxylase, histamine H1 and H2 receptor antagonists, and an H3 receptor agonist. Pharmacol Biochem Behav 90:325-330.

Liu TW, Ma ZG, Zhou Y, Xie JX (2013) Transplantation of mouse CGR8 embryonic stem cells producing GDNF and TH protects against 6-hydroxydopamine neurotoxicity in the rat. Int J Biochem Cell Biol 45:1265-1273.

Liu Z, Cheung HH (2020) Stem cell-based therapies for Parkinson disease. Int J Mol Sci 21:8060.

Lubbe S, Morris HR (2014) Recent advances in Parkinson's disease genetics. J Neurol 261:259-266.

Mendes-Pinheiro B, Teixeira FG, Anjo SI, Manadas B, Behie LA, Salgado AJ (2018) Secretome of undifferentiated neural progenitor cells induces histological and motor improvements in a rat model of Parkinson's disease. Stem Cells Transl Med 7:829-838.

Michel PP, Hirsch EC, Hunot S (2016) Understanding dopaminergic cell death pathways in Parkinson disease. Neuron 90:675-691.

Mine Y, Momiyama T, Hayashi T, Kawase T (2018) Grafted miniature-swine neural stem cells of early embryonic mesencephalic neuroepithelial origin can repair the damaged neural circuitry of Parkinson's disease model rats. Neuroscience 386:51-67.

Monni E, Cusulin C, Cavallaro M, Lindvall O, Kokaia Z (2014) Human fetal striatum-derived neural stem (NS) cells differentiate to mature neurons in vitro and in vivo. Curr Stem Cell Res Ther 9:338-346.

Moriya Y, Itoh M, Okuda S, Yoshizawa AC, Kanehisa M (2007) KAAS: an automatic genome annotation and pathway reconstruction server. Nucleic Acids Res 35:W182-185.

Parmar M, Grealish S, Henchcliffe C (2020) The future of stem cell therapies for Parkinson disease. Nat Rev Neurosci 21:103-115.

Percie du Sert N, Hurst V, Ahluwalia A, Alam S, Avey MT, Baker M, Browne WJ, Clark A, Cuthill IC, Dirnagl U, Emerson M, Garner P, Holgate ST, Howells DW, Karp NA, Lazic SE, Lidster K, MacCallum CJ, Macleod M, Pearl EJ, et al. (2020) The ARRIVE guidelines 2.0: Updated guidelines for reporting animal research. PLoS Biol 18:e3000410.

Pfisterer U, Kirkeby A, Torper O, Wood J, Nelander J, Dufour A, Björklund A, Lindvall O, Jakobsson J, Parmar M (2011) Direct conversion of human fibroblasts to dopaminergic neurons. Proc Natl Acad Sci U S A 108:10343-10348.

Poewe W, Seppi K, Tanner CM, Halliday GM, Brundin P, Volkmann J, Schrag AE, Lang AE (2017) Parkinson disease. Nat Rev Dis Primers 3:17013.

Qian Y, Chen XX, Wang W, Li JJ, Wang XP, Tang ZW, Xu JT, Lin H, Yang ZY, Li LY, Song XB, Guo JZ, Bian LG, Zhou L, Lu D, Deng XL (2020) Transplantation of Nurr1-overexpressing neural stem cells and microglia for treating parkinsonian rats. CNS Neurosci Ther 26:55-65.

Qin H, Zhao A, Ma K, Fu X (2018) Chemical conversion of human and mouse fibroblasts into motor neurons. Sci China Life Sci 61:1151-1167.

Reglödi D, Lubics A, Kiss P, Lengvári I, Gaszner B, Tóth G, Hegyi O, Tamás A (2006) Effect of PACAP in 6-OHDA-induced injury of the substantia nigra in intact young and ovariectomized female rats. Neuropeptides 40:265-274.

Sundberg M, Bogetofte H, Lawson T, Jansson J, Smith G, Astradsson A, Moore M, Osborn T, Cooper O, Spealman R, Hallett P, Isacson O (2013) Improved cell therapy protocols for Parkinson's disease based on differentiation efficiency and safety of hESC-, hiPSC-, and non-human primate iPSC-derived dopaminergic neurons. Stem Cells 31:1548-1562.

Tang Y, Cheng L (2017) Cocktail of chemical compounds robustly promoting cell reprogramming protects liver against acute injury. Protein Cell 8:273-283.

Tang Y, Xiong S, Yu P, Liu F, Cheng L (2018) Direct conversion of mouse fibroblasts into neural stem cells by chemical cocktail requires stepwise activation of growth factors and Nup210. Cell Rep 24:1355-1362.e3.

Tang Y, Meng L, Wan CM, Liu ZH, Liao WH, Yan XX, Wang XY, Tang BS, Guo JF (2017) Identifying the presence of Parkinson's disease using low-frequency fluctuations in BOLD signals. Neurosci Lett 645:1-6.

Thoma EC, Merkl C, Heckel T, Haab R, Knoflach F, Nowaczyk C, Flint N, Jagasia R, Jensen Zoffmann S, Truong HH, Petitjean P, Jessberger S, Graf M, Iacone R (2014) Chemical conversion of human fibroblasts into functional Schwann cells. Stem Cell Reports 3:539-547.

Wang H, Quirion R, Little PJ, Cheng Y, Feng ZP, Sun HS, Xu J, Zheng W (2015) Forkhead box O transcription factors as possible mediators in the development of major depression. Neuropharmacology 99:527-537.

Xu JT, Qian Y, Wang W, Chen XX, Li Y, Li Y, Yang ZY, Song XB, Lu D, Deng XL (2020) Effect of stromal cell-derived factor-1/CXCR4 axis in neural stem cell transplantation for Parkinson's disease. Neural Regen Res 15:112-119.

Yang Y, Wang QQ, Bozinov O, Xu RX, Sun YL, Wang SS (2020) GSK-3 inhibitor CHIR99021 enriches glioma stem-like cells. Oncol Rep 43:1479-1490.

Yasuda S, Kusakawa S, Kuroda T, Miura T, Tano K, Takada N, Matsuyama S, Matsuyama A, Nasu M, Umezawa A, Hayakawa T, Tsutsumi H, Sato Y (2018) Tumorigenicity-associated characteristics of human iPS cell lines. PLoS One 13:e0205022.

Yasuhara T, Kameda M, Sasaki T, Tajiri N, Date I (2017) Cell therapy for Parkinson's disease. Cell Transplant 26:1551-1559.

Ye J, Zhang Y, Cui H, Liu J, Wu Y, Cheng Y, Xu H, Huang X, Li S, Zhou A, Zhang X, Bolund L, Chen Q, Wang J, Yang H, Fang L, Shi C (2018) WEGO 2.0: a web tool for analyzing and plotting GO annotations, 2018 update. Nucleic Acids Res 46:W71-W75.

Yin JC, Zhang L, Ma NX, Wang Y, Lee G, Hou XY, Lei ZF, Zhang FY, Dong FP, Wu GY, Chen G (2019) Chemical conversion of human fetal astrocytes into neurons through modulation of multiple signaling pathways. Stem Cell Reports 12:488-501.

Yu G, Wang LG, Han Y, He QY (2012) clusterProfiler: an R package for comparing biological themes among gene clusters. OMICS 16:284-287.

Yuan Y, Tang X, Bai YF, Wang S, An J, Wu Y, Xu ZD, Zhang YA, Chen Z (2018) Dopaminergic precursors differentiated from human blood-derived induced neural stem cells improve symptoms of a mouse Parkinson's disease model. Theranostics 8:4679-4694.

Zenchak JR, Palmateer B, Dorka N, Brown TM, Wagner LM, Medendorp WE, Petersen ED, Prakash M, Hochgeschwender U (2020) Bioluminescence-driven optogenetic activation of transplanted neural precursor cells improves motor deficits in a Parkinson's disease mouse model. J Neurosci Res 98:458-468.

Zhai Y, Chen X, Yu D, Li T, Cui J, Wang G, Hu JF, Li W (2015) Histone deacetylase inhibitor valproic acid promotes the induction of pluripotency in mouse fibroblasts by suppressing reprogramming-induced senescence stress. Exp Cell Res 337:61-67.

Zhang GL, Wang CF, Qian C, Ji YX, Wang YZ (2021) Role and mechanism of neural stem cells of the subventricular zone in glioblastoma. World J Stem Cells 13:877-893.

Zhang L, Yin JC, Yeh H, Ma NX, Lee G, Chen XA, Wang Y, Lin L, Chen L, Jin P, Wu GY, Chen G (2015) Small molecules efficiently reprogram human astroglial cells into functional neurons. Cell Stem Cell 17:735-747.

Zhao L, Liu JW, Kan BH, Shi HY, Yang LP, Liu XY (2020) Acupuncture accelerates neural regeneration and synaptophysin production after neural stem cells transplantation in mice. World J Stem Cells 12:1576-1590.

Zhou Y, Zhu X, Dai Y, Xiong S, Wei C, Yu P, Tang Y, Wu L, Li J, Liu D, Wang Y, Chen Z, Chen SJ, Huang J, Cheng L (2020) Chemical cocktail induces hematopoietic reprogramming and expands hematopoietic stem/progenitor cells. Adv Sci (Weinh) 7:1901785.

Zhu Y, Huang R, Wu Z, Song S, Cheng L, Zhu R (2021) Deep learning-based predictive identification of neural stem cell differentiation. Nat Commun 12:2614.

P-Reviewers: Schweitzer J, Laffita-Mesa JM; C-Editor: Zhao M; S-Editors: Yu J, Li CH; L-Editors: Iwabuchi S, Yu J, Song LP; T-Editor: Jia Y